Reverse-time migration using the energy imaging condition in TTI media

Alejandro Cabrales-Vargas

ABSTRACT

I extend my previous work about the energy imaging condition for anisotropic reverse-time migration to tilted-transverse isotropic media. Synthetic examples show the feasibility of this implementation.

INTRODUCTION

This report constitutes the follow-up of a previous report (Cabrales-Vargas, 2016) where I implemented the energy imaging condition (EIC) in vertical-transverse isotropic (VTI) media. Similar to its isotropic counterpart, EIC can be used to enhance either the tomographic component (applicable to improving the full waveform inversion gradient for cycle skipping reduction) or the reflectivity component of the image (Whitmore and Crawley, 2012; Rocha et al., 2016a,b) for imaging purposes.

In this report I first introduce the EIC for tilted-trasverse isotropic (TTI) media. Next, I show the numerical results obtained on the BP TTI 2-D synthetic model. Finally, I present the conclusions of this work.

METHOD

In isotropic acoustic media (e.g. Rocha et al., 2016a) the EIC can be derived from the energy function of the acoustic wave equation, which is defined as

$$E(t) = \int_\Omega \left[\frac{1}{v^2} \left(\frac{\partial u}{\partial t} \right)^2 + \|\nabla u\|^2 \right] d\mathbf{x} = \int_\Omega \|\Box u\|^2 d\mathbf{x}, \tag{1}$$

where $E(t)$ is the energy of the acoustic wave equation, u is the propagation wavefield. From this expression Rocha et al. (2016a) derived the EIC as

$$I(\mathbf{x}) = \sum_t \Box S(\mathbf{x}, t) \cdot \widetilde{\Box} R(\mathbf{x}, t), \tag{2}$$

where S and R are the source wavefield and the receiver wavefield, respectively. The operator $\Box$ represents a space-time gradient (also known as *D'Alembertian*), given in three-dimensional space-time by

$$\Box = \left(\frac{1}{v} \frac{\partial}{\partial t}, \quad \frac{\partial}{\partial x}, \quad \frac{\partial}{\partial z} \right), \tag{3}$$

and the operator $\widetilde{\Box}$ is a modified space-time gradient given by

$$\widetilde{\Box} = \left(\cos(2\gamma_c)\frac{1}{v}\frac{\partial}{\partial t}, \quad \frac{\partial}{\partial x}, \quad \frac{\partial}{\partial z}\right), \tag{4}$$

where γ_c represents a cut-off angle that rejects seismic events in the neighborhood of such value for the reflection angle. For example, setting $\gamma_c = 0°$ preserves the reverse-time migration (RTM) tomographic component and rejects reflections in the neighborhood of zero degrees. On the contrary, setting $\gamma_c = 90°$ rejects most of the tomographic component and preserves the reflectivity component, similar to the Laplacian low-cut filter (Rocha et al., 2016a).

For the TTI case I utilize the anisotropic wave equations proposed by Zhang et al. (2011),

$$\frac{1}{v^2}\frac{\partial^2 \mathbf{p}}{\partial t^2} = \mathbf{B}\mathbf{G}_2\mathbf{p}, \tag{5}$$

where $\mathbf{p} = [p, r]^T$ is the stress vector with horizontal component, p, and vertical component, r, matrices $\mathbf{B}$ and $\mathbf{G}_2$ are given by

$$\mathbf{B} = \begin{bmatrix} 1+2\epsilon & \sqrt{1+2\delta} \\ \sqrt{1+2\delta} & 1 \end{bmatrix} \tag{6}$$

and

$$\mathbf{G}_2 = \begin{bmatrix} G_{xx} & 0 \\ 0 & G_{zz} \end{bmatrix}, \tag{7}$$

where $G_{xx} = G_x^T G_x$ and $G_{zz} = G_z^T G_z$, and

$$\begin{aligned} G_x &= D_x COS(\theta) - D_z SIN(\theta), \\ G_z &= D_z SIN(\theta) + D_z COS(\theta), \end{aligned} \tag{8}$$

where ϵ and δ are the Thomsen parameters, D_x and D_z represent the first order derivative operators with respect x and z respectively, G_x and G_z constitute the first order derivatives after axis rotation by the dip angle field θ, and $SIN(\theta)$ and $COS(\theta)$ are the corresponding trigonometric functions with their elements arranged as diagional matrices. The corresponding transpose derivatives are given by

$$\begin{aligned} G_x^T &= COS(\theta)^T D_x^T - SIN(\theta)^T D_z^T, \\ G_z^T &= SIN(\theta)^T D_z^T + COS(\theta)^T D_z^T. \end{aligned} \tag{9}$$

Using Equations 8 and 9 we ensure that Equation 5 remains stable by keeping matrix $\mathbf{G}_2$ symmetric and negative definite (Zhang et al., 2011). In the current implementation I employ central differences and staggered grids for the derivative operators D_x and D_z, followed by linear interpolation to the original grid. Logically, D_x^T and D_z^T are implemented by applying the adjoint of the interpolation operator, followed by the adjoint of the derivative operator.

The definition of the TTI EIC beginning from the energy of the TTI wave equation (Equation 5) is similar to the VTI case (Cabrales-Vargas, 2016). In such a case the energy of the VTI wave equation is given by

$$E(t) = \int_\Omega \left\{ \frac{1}{v^2}[\|\mathbf{\Lambda}^{-\frac{1}{2}}\mathbf{Y}\|^2\dot{\mathbf{p}} + \|\mathbf{D}\mathbf{p}\|^2 \right\} d\mathbf{x} = \int_\Omega \|\Box\mathbf{p}\|^2 d\mathbf{x}, \tag{10}$$

where the columns of matrix $\mathbf{Y}$ are the eigenvectors of matrix $\mathbf{B}$, and the diagonal of matrix $\mathbf{\Lambda}$ contains the eigenvalues of matrix $\mathbf{B}$. Such matrices are obtained from the diagonalization process: $\mathbf{B} = \mathbf{Y}^T\mathbf{\Lambda}\mathbf{Y}$. Matrix $\mathbf{D}$ represents the first derivative operator, defined as

$$\mathbf{D} = \begin{bmatrix} \frac{\partial}{\partial x} & 0 \\ 0 & \frac{\partial}{\partial z} \end{bmatrix}. \tag{11}$$

With these definitions the space-time gradient for the VTI wave equation becomes a matrix-like operator defined by

$$\Box = \left(\frac{1}{v}\mathbf{\Lambda}^{-\frac{1}{2}}\mathbf{Y}\frac{\partial}{\partial t}, \mathbf{D} \right) \tag{12}$$

and the modified version with cut-off angle

$$\widetilde{\Box} = \cos(2\gamma_c)\left(\frac{1}{v}\mathbf{\Lambda}^{-\frac{1}{2}}\mathbf{Y}\frac{\partial}{\partial t}, \mathbf{D} \right). \tag{13}$$

Therefore, the VTI EIC can be written as

$$\begin{aligned} I(\mathbf{x};\gamma_c) = &\sum_t \Box\mathbf{p}_S \cdot \widetilde{\Box}\mathbf{p}_R = \\ &\sum_t \left\{ \cos(2\gamma_c)\frac{1}{v^2}[\mathbf{\Lambda}^{-\frac{1}{2}}\mathbf{Y}\dot{\mathbf{p}}_S] \cdot [\mathbf{\Lambda}^{-\frac{1}{2}}\mathbf{Y}\dot{\mathbf{p}}_R] + [\mathbf{D}\mathbf{p}_S] \cdot [\mathbf{D}\mathbf{p}_R] \right\}. \end{aligned} \tag{14}$$

For TTI we substitute $\mathbf{G}$ for $\mathbf{D}$,

$$E(t) = \int_\Omega \left\{ \frac{1}{v^2}[\|\mathbf{\Lambda}^{-\frac{1}{2}}\mathbf{Y}\|^2\dot{\mathbf{p}} + \|\mathbf{G}\mathbf{p}\|^2 \right\} d\mathbf{x} = \int_\Omega \|\Box\mathbf{p}\|^2 d\mathbf{x}, \tag{15}$$

where $\mathbf{G}$ is given as

$$\mathbf{G} = \begin{bmatrix} G_x & 0 \\ 0 & G_z \end{bmatrix} \tag{16}$$

The corresponding TTI EIC thus becomes

$$\begin{aligned} I(\mathbf{x};\gamma_c) = &\sum_t \Box\mathbf{p}_S \cdot \widetilde{\Box}\mathbf{p}_R = \\ &\sum_t \left\{ \cos(2\gamma_c)\frac{1}{v^2}[\mathbf{\Lambda}^{-\frac{1}{2}}\mathbf{Y}\dot{\mathbf{p}}_S] \cdot [\mathbf{\Lambda}^{-\frac{1}{2}}\mathbf{Y}\dot{\mathbf{p}}_R] + [\mathbf{G}\mathbf{p}_S] \cdot [\mathbf{G}\mathbf{p}_R] \right\}. \end{aligned} \tag{17}$$

The image normalization employed in the VTI case (Cabrales-Vargas, 2016) is applicable for TTI EIC. I use such normalization in the numerical examples presented in the next section.

SYNTHETIC EXAMPLES

I compare the result of the EIC with the crosscorrelation imaging condition (CIC) by applying anisotropic RTM to one half of the BP TTI synthetic dataset (Figure 1(a)).

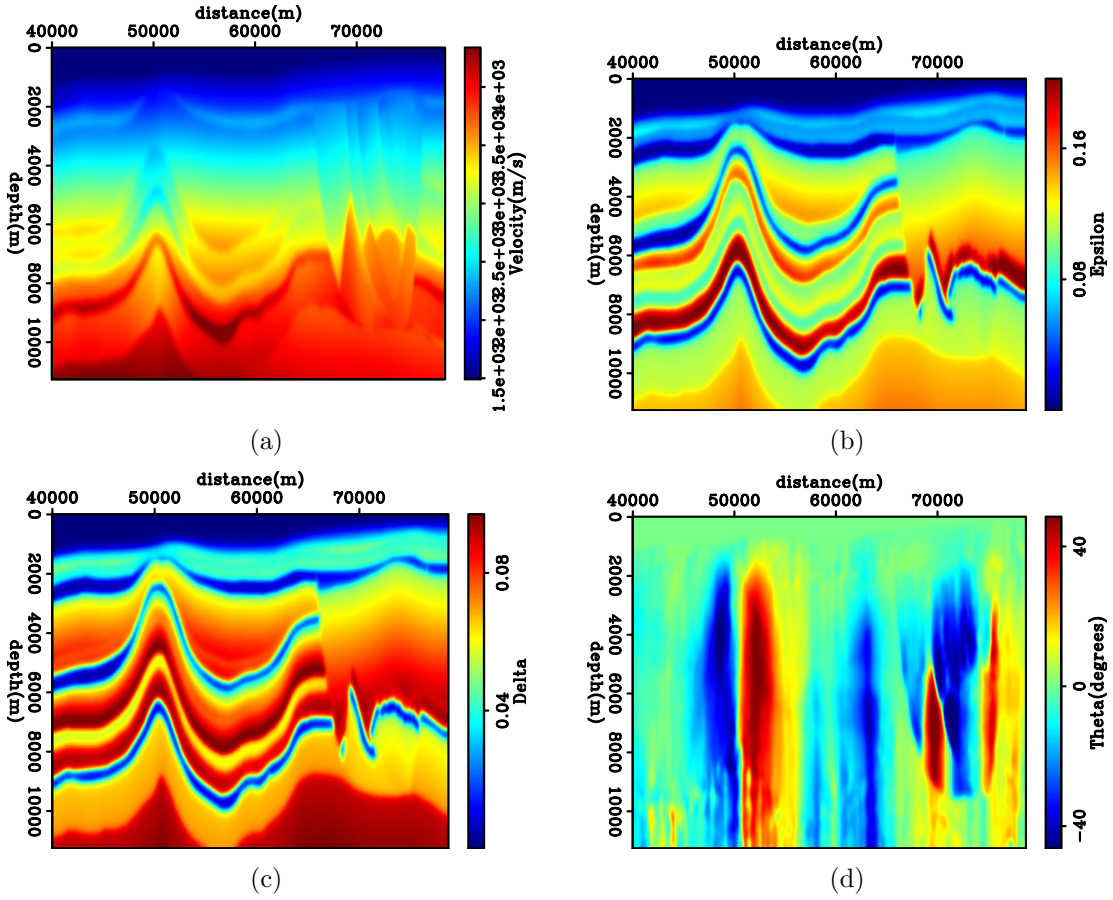

Figure 1: BP TTI synthetic model, after smoothing: (a) Velocity; (b) Epsilon; (c) Delta; (d) Theta (dip) [**ER**].

Figure 2 shows the TTI-RTM result using the CIC. The seismic events are obscured by the tomographic component of the RTM image. Applying the EIC with $\gamma_c = 0°$ (Figure 3) we can preserve such tomographic component. Figures 2 and 3 are very similar, but closer examination reveals that in fact, using CIC the reflections are simply *obscured*, while using EIC for $\gamma_c = 0°$ the reflections become *attenuated*. Figures 4 and 5 show the corresponding sections after the application of a Laplacian filter, confirming the last argument. The oceanic floor reflector persists because it encompasses a wide reflection angle range, whereas the cut-off angle has the rejection band confined to a small threshold, in this case around 0°. Rocha et al. (2016a) discuss the potential benefit of attenuating the reflectivity while preserving the tomographic component in the computation of the full-waveform inversion gradient, thus reducing the susceptibility to cycle skipping.

Figure 6 shows the result of the EIC setting $\gamma_c = 90°$ to preserve reflectivity, to

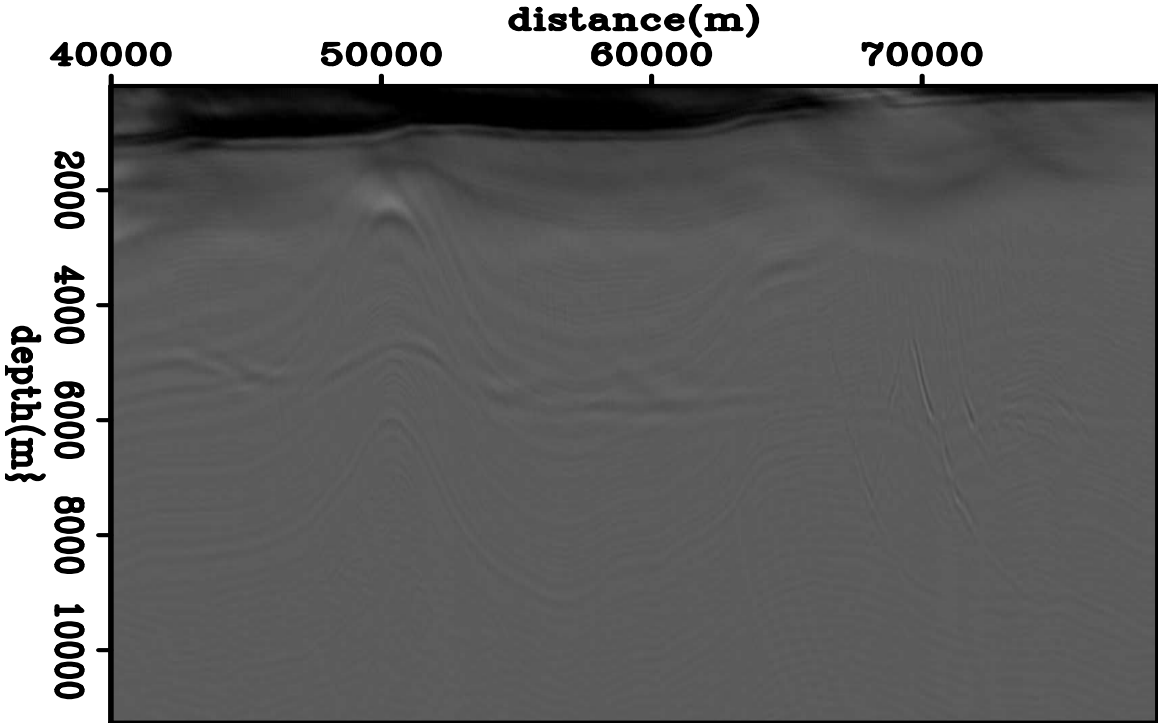

Figure 2: TTI reverse-time migration using CIC [**CR**].

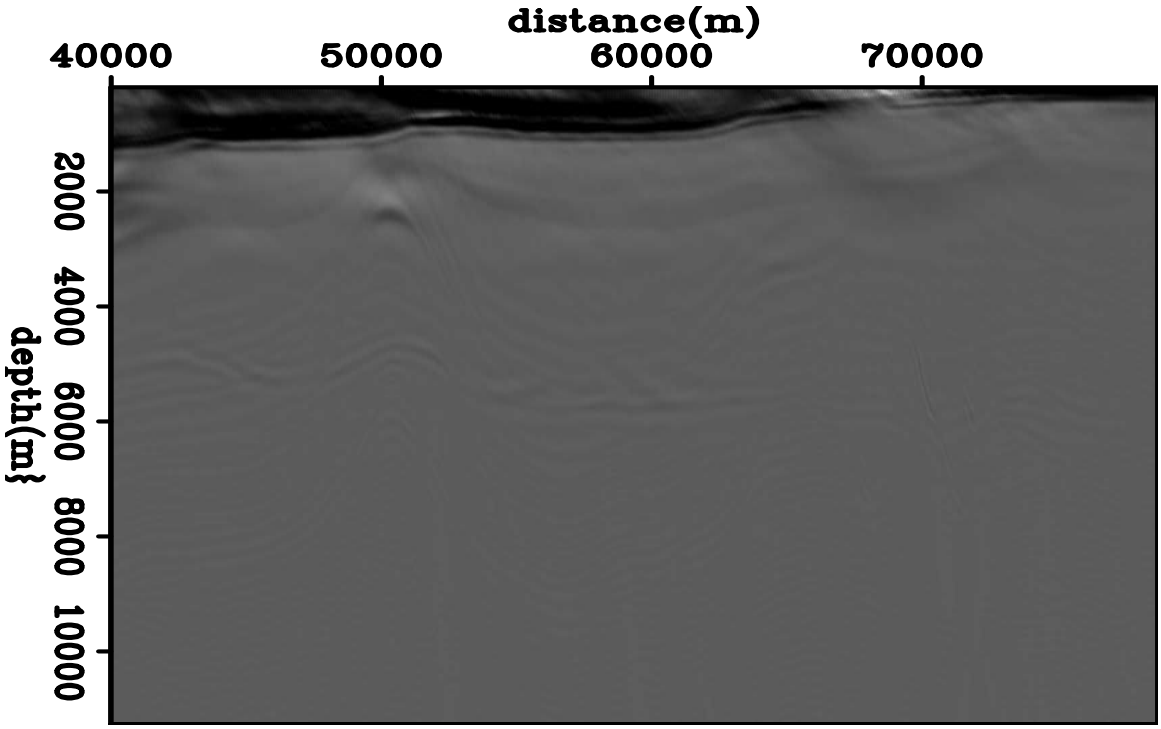

Figure 3: TTI reverse-time migration usinf EIC with $\gamma_c = 0^\circ$ [**CR**].

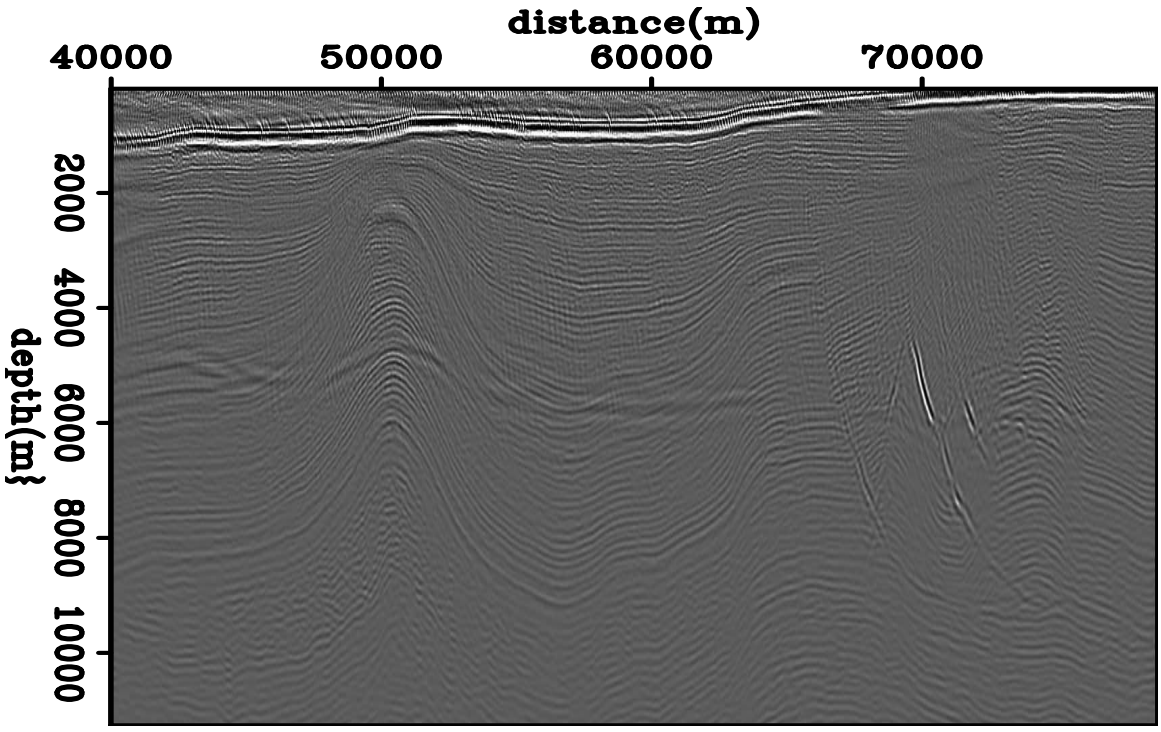

Figure 4: TTI reverse-time migration using CIC, after the application of a Laplacian filter [**CR**].

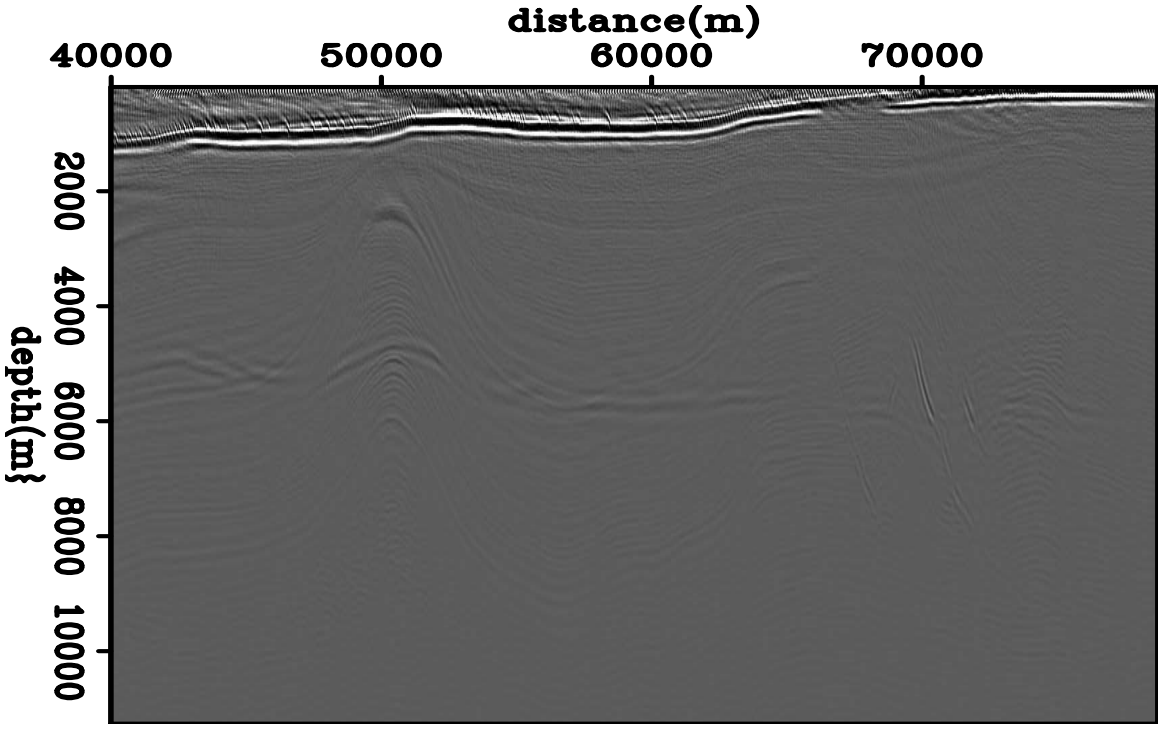

Figure 5: TTI reverse-time migration usinf EIC with $\gamma_c = 0°$, after the application of a Laplacian filter [**CR**].

be compared with Figure 4. This EIC section still exhibits remaining artifacts in the shallow part, which are absent in the filtered version of CIC. On the other hand, the Laplacian filter slightly affects the continuity of some shallow events near the ocean bottom. In contrast to the acoustic case (Rocha et al., 2015, 2016a), it is possible that in anisotropic propagation, γ_c values other than 90° might give better results in attenuating the tomographic component. In fact, the EIC offers the flexibility to choose among different rejection angles, but additional research is needed to determine the optimum value of γ_c without relying on trial and error.

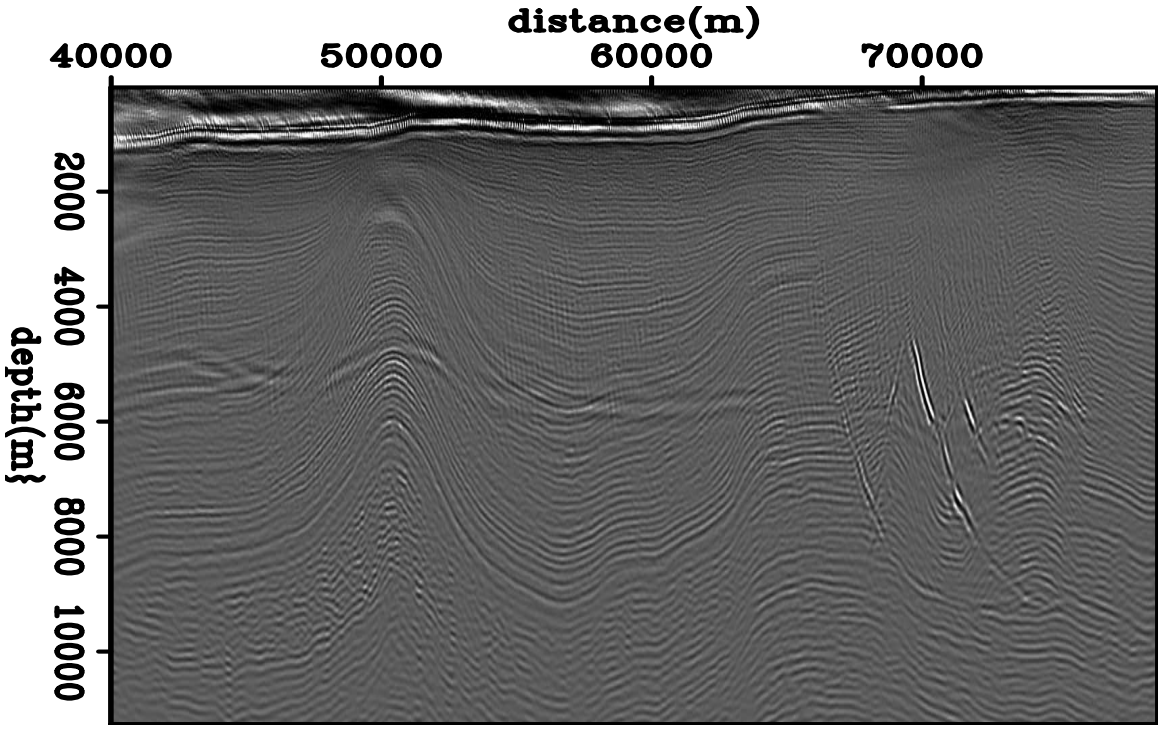

Figure 6: TTI reverse-time migration usinf EIC with $\gamma_c = 90°$ [**CR**].

CONCLUSION

I derived a TTI energy imaging condition from the VTI case presented in the previous SEP report. The numerical results show satisfactory preservation of the tomographic component when setting $\gamma_c = 0°$. Preservation of the reflectivity component was less than optimum, possibly because the anisotropic case might require to set γ_c to angle values other than 90°. Therefore, additional research is needed to determine the optimum cut-off angle.

ACKNOWLEDGEMENT

I would like to thank the SEP sponsors for their support, and to British Petroleum for the synthetic BP TTI model. I also extend special thanks to Petróleos Mexicanos

for the financial support.

REFERENCES

Cabrales-Vargas, A., 2016, Reverse-time migration using the energy imaging condition in isotropic and vti media: SEP-Report, **163**, 77–90.

Rocha, D., N. Tanushev, and P. Sava, 2015, Acoustic wavefield imaging using the energy norm: SEG Technical Program Expanded Abstracts 2015, 4085–4090.

———, 2016a, Acoustic wavefield imaging using the energy norm: Geophysics, **81**, no. 4, S151–S163.

———, 2016b, Isotropic elastic wavefield imaging using the energy norm: Geophysics, **81**, no. 4, S207–S219.

Whitmore, N. and S. Crawley, 2012, Applications of RTM inverse scattering imaging conditions: SEG Technical Program Expanded Abstracts 2012, 1–6.

Zhang, Y., H. Zhang, and G. Zhang, 2011, A stable TTI reverse time migration and its implementation: Geophysics, **76**, no. 3, WA3–WA11.